

Surface wave excitations and backflow effect over dense polymer brushes

Sofia Biagi,^{1,2,*} Lorenzo Rovigatti,^{2,3} Francesco Sciortino,^{2,4} and Chaouqi Misbah¹

¹*Université Grenoble Alpes/CNRS UMR 5588, LIPhy, 38041 Grenoble, France*

²*Dipartimento di Fisica, Sapienza-Università di Roma, Piazzale A. Moro 5, 00185 Roma, Italy*

³*Faculty of Physics, University of Vienna, Boltzmannngasse 5, A-1090 Vienna, Austria*

⁴*Istituto Sistemi Complessi (ISC), Via dei Taurini 19, 00185 Roma, Italy*

(Dated: July 1, 2021)

Polymer brushes are increasingly used to tailor surface physicochemistry for various applications such as wetting, adhesion of biological objects, implantable devices, etc. We perform Dissipative Particle Dynamics simulations to study the behavior of dense polymer brushes under flow in a slit-pore channel. We discover that the system displays flow inversion at the brush interface for *several* disconnected ranges of the imposed flow. We associate such phenomenon to collective polymer dynamics: a wave propagating on the brush surface. The relation between the wavelength, the amplitude and the propagation speed of the flow-generated wave is consistent with the solution of the Stokes equations when an imposed traveling wave is assumed as boundary condition (the famous Taylor’s swimmer).

PACS numbers: 47.56.+r, 47.63.-b, 82.35.Lr, 87.15.H-

Polymer brushes are passive media whose great variety allows for a rich range of applications. Brushes with different mechanical properties can be created by grafting simple polymers, block copolymers or polymer stars to a solid substrates or to an interface between two liquids. They are exploited for colloid stabilization [1–3], as lubricant layers [4–6], as adhesion regulators [7, 8] and for biomedical technological applications. A holdover interest in these systems is indeed motivated by the discovery that the inner surface of various mammalian organs is decorated by densely grafted macromolecules. For example, the lumen of blood vessels is protected by a hundred nanometers thick polymer brush mainly made of glucose and its compounds. Such an heterogeneous network is called “glycocalyx” [9, 10]. Research on the glycocalyx dynamics is central for a complete understanding of the blood circulatory system and, hopefully, to shed light on the initial stages of diseases like thrombosis and atherosclerosis [11]. Understanding glycocalyx is also relevant to the polymeric coatings of lungs, small intestine and uterus [12–14].

Most theoretical studies have attempted to model polymer brushes as porous media described by Brinkman-type equations [15] or as elastic media composed of very rigid fibers [16]. In this Letter, we report an analysis of a polymer brush whose features approach the glycocalyx system and for which the set up conditions recall the microcirculation frame [17]. We focus on dense polymer brushes under flow, in which the brush is modeled as a collection of individual polymers. We implement a Dissipative Particle Dynamics (DPD) code [18–21] with explicit solvent and numerically analyse the dynamics of a linear flexible homo-disperse polymer brush subdued to a simple liquid parabolic flow in a slit-pore geometry. The coarse-grained DPD procedure applies to both solvent molecules and polymer monomers, offering the pos-

sibility to (i) reproduce hydrodynamic interactions while retaining a detailed view of the brush dynamics on the scale of the coarse-grained monomers; (ii) access both the polymer dynamics, influenced by the imposed flow, and the flow field, perturbed by the presence and motion of the brush.

Recent studies of polymer brushes under flow [22–24] have highlighted an unexpected behavior in the velocity profile in the vicinity of the brush surface. These studies have reported that the velocity field reverses on increasing the flow field and have tentatively associated such result to the peculiar dynamics of the single polymer undergoing a cyclic motion of stretching, elongation and recoiling. Stimulated by these studies we have undertaken a numerical investigation exploring a very large range of imposed flow, aiming at quantifying the conditions under which the physical properties of the brush couple with the hydrodynamic properties of the solvent to produce flow inversion. As presented below, we discover (i) that flow inversion appears in distinct regions of imposed flow values; (ii) that every time flow inversion is observed a surface wave appears, stressing that such backflow is strongly associated to a collective (as opposed to single) polymer dynamics; (iii) that the wave properties are consistent with predictions derived by Taylor in his seminal study on pusher microswimmers [25]. Thus, our work presents a new interpretation for the flow inversion phenomenon and provide a novel connection between two separated fields: polymer brushes under flow and microswimmers.

A short description of the DPD methodology and of its application to the slit-pore geometry is reported in the Supplementary Informations (S.I., Sect.1). Here we recall that we simulate a parallelepiped box of sides L_x , L_y , L_z , with polymers chains composed by 40 (coarse-grained) monomers grafted at $z = 0$ (see Fig. 1). Our

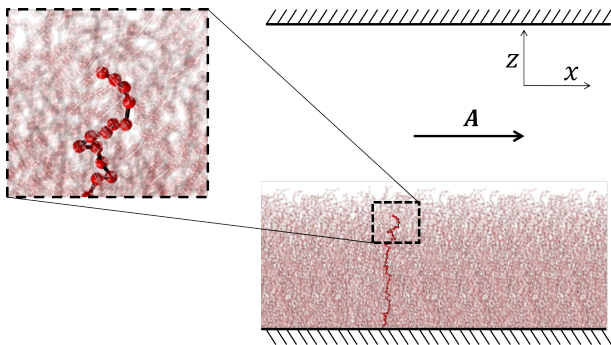


FIG. 1. Schematic representation of the investigated slit-pore system. Polymers are grafted at the bottom wall $z = 0$ while the rest of the channel is occupied by solvent particles. An additional sketch is provided with a zoom on a typical chain (highlighted in red). The constant acceleration A is applied along the x axis to all solvent particles.

discussion pertains simulations in a box of size $L_x = 30$, $L_y = 5$ and $L_z = 50$, in units of r_c (see S. I. for definitions). We remark that we observe the same phenomenology we are going to present also in considerably bigger boxes ($L_x = 360$, $L_y = 20$ and $L_z = 150$). However, for the sake of computational time and memory capacity, the systematic analysis has been conducted in a smaller channel. The equilibrium distance between neighbour monomers in a chain is $0.89r_c$. The grafting density $\sigma_{graft} \equiv N_{ch}/(L_x L_y)$ with N_{ch} the number of chains composing the brush, being $\sigma_{graft} = 1.5$, corresponds to the condition of dense brush. Periodic boundary conditions are applied along the x and y directions. In the channel, a flow is imposed by applying a constant acceleration $A\hat{x}$ to all solvent particles, resulting in a parabolic velocity profile along the z direction. The strength of the velocity is controlled by the value of A . In the following, instead of A , we will use the so-called Weissenberg number $Wi \equiv \frac{t_{brush}}{t_{flow}}$, which provides an adimensional information on the relative timescale of the unperturbed brush dynamics (t_{brush}) over the inverse of the averaged shear rate inside the channel (t_{flow}). Specific values for all parameters and their units and a detailed discussion of the A dependence of t_{flow} are reported in the S.I., Sect.1,3.

The velocity profile $v_x(z)$, calculated by averaging the x -component of the velocity for each solvent particle as a function of its position z , is shown in Figs. 2.(a)-(b) for two Wi values, providing two typical examples. As expected, the functional shape of $v_x(z)$ in the region around the largest velocity v_{max} is well represented by a parabolic function with the expected amplitude. In all cases, the parabolic function predicts that v_x vanishes when z approaches the brush height h , suggesting that, for all studied Wi , the presence of a dense polymer brush restricts the pore by an amount equivalent to h . The ve-

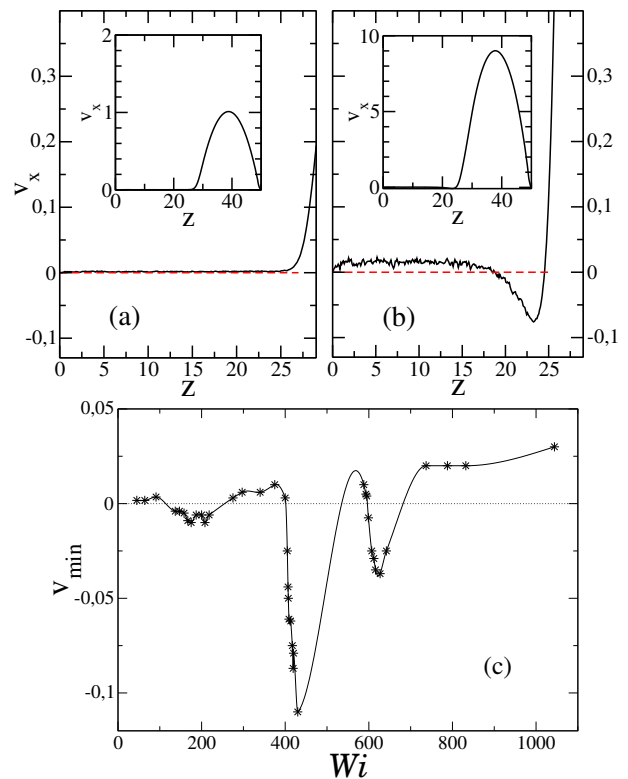


FIG. 2. Panels (a) and (b) show the velocity profile in the region where the brush is set and they are a zoom of the respective insets. In both cases, corresponding to (a) $Wi = 45$ and (b) $Wi = 418$, the profile is parabolic around v_{max} . In (a) no backflow is registered, while in (b) the flow inversion at $z \sim h$ is evident. Panel (c) reports the minimum value v_{min} of the $v_x(z)$ profile for different Wi (symbols). The line is a guide for the eye. It is possible to recognize three regions for which v_{min} assumes a negative value, signalling the presence of a backward flow.

locity profile in the region $z < h$, i.e. the region occupied by the brush, is particularly interesting. In some cases, e.g. the one of Fig. 2.(a), the fluid velocity inside the brush is small, consistent with a picture in which the hydrodynamic interactions are effectively screened by the presence of the polymer layer. In other cases, as shown in Fig 2.(b), the velocity profile exhibits a flow inversion at the interface between the brush and the bulk, e.g. around $z \sim h$, as previously documented for an analogous system [24] as well as when the solvent is replaced by a polymer melt in [22, 23]. In these previous studies, the onset of flow inversion was associated to the point at which the shear rate exceeds a certain threshold [24]. Oppositely, we find that flow inversion takes place in different distinct disconnected windows of Wi values. Indeed, we uncover at least three different windows of flow intensities in which a backflow is observed. In between these regions the velocity profile at $z \sim h$ resembles the one in Fig. 2.(a). Fig. 2.(c) shows the minimum value v_{min} of the profile $v_x(z)$ near the surface of the polymer brush,

as function of Wi . By this definition, flow inversion is observed when $v_{min} < 0$. The identified three back-flow regions fall around $Wi \sim 200, 400, 600$.

In the previously mentioned papers [22–24] it was argued that the backflow is a consequence of the grafted single chain dynamics, performing a recursive imperfect cycle composed of: tilting, elongation and recoiling. Indeed, an elongated chain (and thus exposed to flow) is dragged by the shear stress along the flow direction and then recoiled back by entropic forces. By examining the polymer trajectories we confirm the presence of such recursive motion (see movie in the S.I., Sect.4) for all Wi values, but such cyclic motion is found to be independent on the presence of the back-flow effect. Hence, such single-polymer motion can not explain the onset of flow inversion.

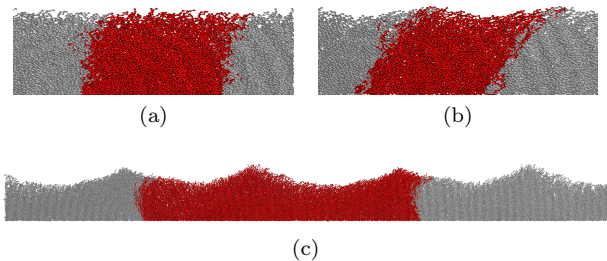


FIG. 3. Sketches of the whole brush, corresponding to (a) $Wi = 91$ and (b) $Wi = 418$. In (a) the brush surface is basically flat, while in (b) the surface is modulated by a traveling wave with $\lambda \sim L_x = 30$, $\nu = 0.077$ and $b = 1.18$. In (c) a snapshot for a larger studied systems ($L_x = 180$, $L_y = 5$ and $L_z = 150$) with a surface wave with multiple crests of wavelength $L_x/2 \approx 90$ ($Wi = 340$). We show the central box (in red) and the two nearest replicas (in grey) to highlight the periodic nature of the waves.

Investigating space and time correlations among different polymers, we discover a wave traveling over the brush surface in the same direction as the imposed flow. The wave arises *only* when back-flow is present, suggesting a strong association between the surface wave and the capability of the brush to produce an inversion of the flow velocity around $z \sim h$. A visual observation of the brush and of its dynamics nicely show the collective behavior of the polymers: Fig. 3.(a),(b) show a typical frame for two generic cases of absence and presence of flow inversion. Videos of the time dependence of the brush are available in the S.I., Sect.4. We find that this traveling wave has a clear spatial periodicity of the order of the simulation box and a non-negligible amplitude. We characterize such surface wave evaluating its frequency ν , wavelength λ and oscillation amplitude b . To do so we define the brush surface $S(x, t)$ as the position of the furthest monomer from the grafting wall occupying at time t the coordinate x , averaged over all y . The power-spectrum of the time Fourier transform of

$S(x_0, t)$ (for an arbitrary x_0 value, inset of Fig. 4.(a)) displays, in all cases in which a flow inversion is observed, a sharp peak at a given frequency (Fig. 4.(a)) that we associate to ν . In some cases a much less intense peak is also observed at 2ν . Fourier transforming the signal $S(x, t_0)$ in real space for an arbitrary t_0 and averaging over all configurations provides a quantification of the wavelength λ . As shown in Fig. 4.(b), for all cases in which a flow inversion is present we find, as in the time domain, a dominant contribution from the longest λ that can propagate in a period system of size L_x and from its second harmonic (e.g. from wavenumbers k equal to $\frac{2\pi}{L_x}$ and $\frac{4\pi}{L_x}$). Fig. 4.(c) shows the Wi dependence of ν for systems with the same L_x (e.g. same λ). In each of the three disconnected regions of Wi values where flow inversion is present, ν increases approximately linearly with Wi . Finally, we define the wave amplitude b as the standard deviation of $S(x, t)$ and the wave average height as $\bar{S} \equiv \langle S(x, t) \rangle$.

We stress that wave propagation is observed also in systems of different L_x . We find that increasing the length L_x and the width L_z of the channel, multiple wave crests can be displayed (in Fig. 3.(c) an example). This suggests that the finite size of the simulation box exerts a cutting on the density of states, making it possible to observe only waves with wavenumbers which are integer multiple of $2\pi/L_x$. Further details on finite size effects are reported in the S.I., Sect.5.

To dig into the reasons why a flow inversion is observed every time there is a wave propagation, we recall the derivation provided by Taylor [25], dated back to 1951, to explain the mobility of pusher microswimmers. In his seminal paper, Taylor determines analytically the self-propelling velocity V_{Taylor} , at low Reynolds number, of an infinite two dimensional sheet whose profile is a sinusoidal wave traveling with (opposite) velocity U :

$$|V_{Taylor}| = \frac{2\pi^2 b^2}{\lambda^2} \left(1 - \frac{19}{4} \frac{\pi^2 b^2}{\lambda^2} \right) U, \quad (1)$$

where b and λ are, respectively, the amplitude and wavelength of the sinusoidal wave. By associating the two dimensional sheet with the brush surface, the wave velocity of the sheet with the wave velocity of the brush surface and the self-propelling velocity of the sheet with the opposite velocity of the solvent at the brush surface v_{min} , Taylor's expression provides a precise relation between the parameters entering in the wave phenomenon and the parameters controlling the flow inversion. In Fig. 5 we show, for each set of b , λ and U values associated to a specific Wi value giving flow inversion, both $|V_{Taylor}|$ (from Eq. (1)) and $|v_{min}|$. All the trends of the $|v_{min}|$ behavior are perfectly recovered by the self-propelling velocity of a Taylor's micro-swimmer, suggesting that indeed the elastic brush can be considered as an anchored micro-swimmer, unable to move but able to propel the surrounding liquid.

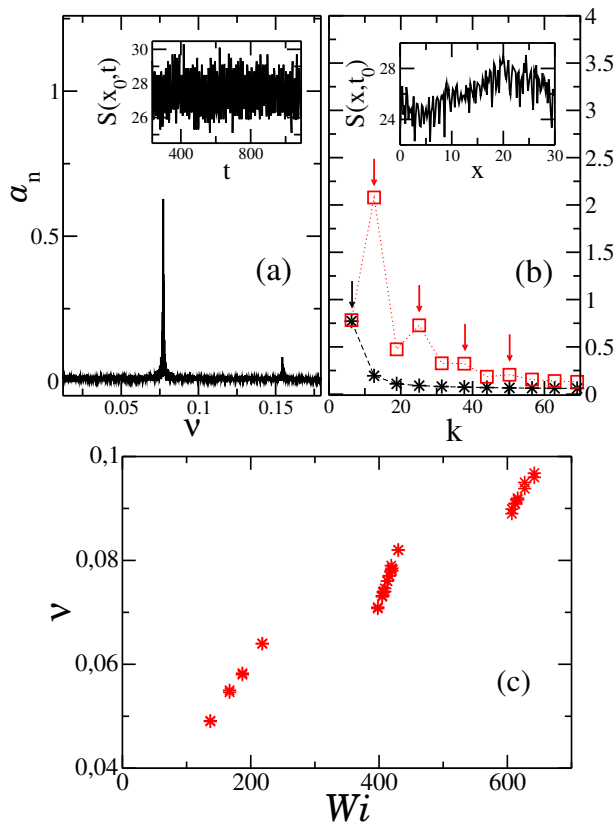


FIG. 4. Fourier power-spectra: (a) in the frequency domain ν for the signal $S(x_0, t)$, (b) in the wavenumber domain $k = 2\pi/\lambda$ for the signal $S(x, t_0)$ (red squares indicate the spectrum in a bigger system $L_x = 180$, $L_y = 5$ and $L_z = 150$). In both cases the first and second harmonics are visible. The two insets show typical signals in real space. Panel (c) shows the first harmonic frequencies corresponding to the Wi giving backflow. Such frequencies monotonically increase.

As a last consideration, we investigate possible origins of the surface wave. Our results suggest that the wave propagation arises from hydrodynamics interactions synchronising polymers, in a sort of metachronal motion. A “metachronal wave” is known to develop in ciliated systems, namely flat surfaces covered by a regular matrix of equally spaced flexible filaments [26, 27]. Exposed to flow, filaments do not interact directly, but thanks to hydrodynamics interactions, after some transient time, they reach a synchronized state with a regular phase shift between subsequent filament rows. However, in those cases, the matrix is composed by active matter elements and the sequence of configurations they assume is assigned *a priori*. On the contrary, polymer brushes are passive media. Different approaches have been developed to model wave formation on passive media such as crop canopies (because of flowing wind) or aquatic vegetations (because of water flow), but they require also the inertial term of Navier-Stokes equations to account for the instability initiating the surface modulation [28, 29]. However, we can

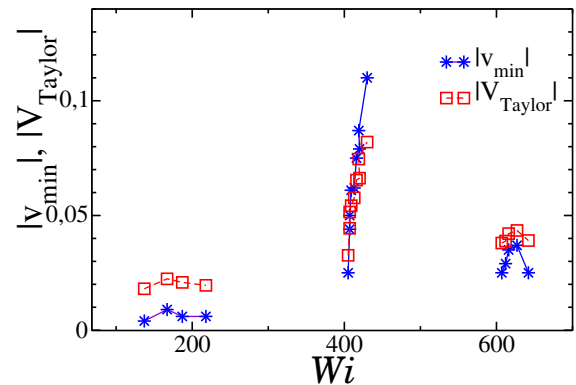


FIG. 5. The mapping between the absolute value of the velocity profile minimum $|v_{min}|$ (stars) and the velocity V_{Taylor} obtained by inserting in Eq. (1) the wave amplitude b , the wavelength λ and the speed velocity $U = \lambda\nu$ evaluated for the brush surface wave at the given Wi .

consider the brush to be an elastic medium. Therefore, the presence of a wave suggests that a possible resonance effect may arise between the shear rate $\dot{\gamma}$ at the brush surface, produced by the imposed flow, and the frequency ν_{com} associated to the time scale of relaxation from the elastic compression of the whole brush [30]. This would point to one threshold value of Wi beyond which surface oscillations are observed, which is not consistent with the findings of waves in at least three different Wi regions. To clarify this inconsistency, we show in Fig. 6 the shear rate $\dot{\gamma}$ estimated by a linear fit of the velocity profile $v_x(z)$ at the brush surface $z \sim S$, as a function of A . We ascribe the striking non-linear behaviour of $\dot{\gamma}$ vs. A to the compression of the brush at high imposed flow. We also find a significant dependence of the brush elastic compression properties on A , suggesting the possibility of multiple intersections of the two quantities $\dot{\gamma}$ and ν_{com} (and hence multiple resonances and multiple regions of flow inversion) on varying A or, equivalently, Wi (see S.I., Sect.2).

In summary, we have discovered for dense polymer brushes under flow a well-characterized surface traveling wave, which appears in all cases of back-flow and it is not present in the other ones, providing a novel picture of the flow-inversion phenomenon, associated to a collective motion of the whole brush rather than to a single chain dynamics. We have also observed a striking and unexpected similarity in the relation between the wave velocity and the back-flow velocity in the case of flow in passive polymer brushes and the same relation for the case of active pusher microswimmers [25].

Discussions with prof. Philippe Peyla are kindly acknowledged. C.M. and S.B. also acknowledge financial support from CNES (Centre National d’Etudes Spatiales) and ESA (European Space Agency). L.R. acknowledges support from the Austrian Research Fund (FWF) through his Lise-Meitner Fellowship M 1650-N27.

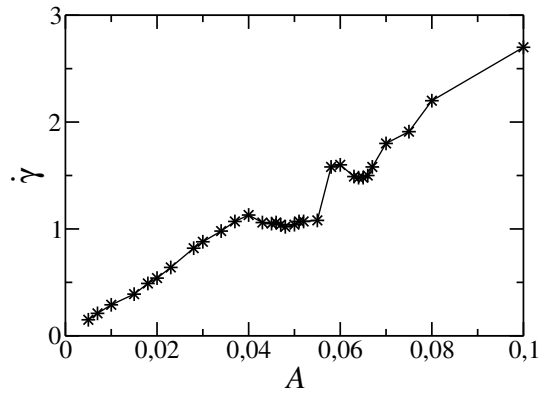


FIG. 6. The shear rate $\dot{\gamma}$ measured from a linear fit of the velocity profile $v_x(z)$ at the brush surface $z \sim S$ for different flow intensities A .

Supplementary Information

1. DPD METHODOLOGY

DPD is a coarse-grained Molecular Dynamics method. It was introduced by Hoogerbrugge and Koelman in 1992 [18] to simulate isothermal Navier-Stokes equations and it has been recently recognized that it can be successfully applied to any mesoscopic scale [31]. In the spirit of DPD, the simulated particle does not correspond to a single molecule, but rather to a significant large *cluster* of them. Each of the N point-like particles evolves in time according to Newton's equations

$$m_i \dot{\vec{v}}_i = \sum_{j \neq i}^N \vec{F}_{ij} = \sum_{j \neq i}^N (\vec{F}_{ij}^C + \vec{F}_{ij}^D + \vec{F}_{ij}^S) \quad (2)$$

that we solve by using the velocity Verlet algorithm [32]. Observables are then calculated as averaged all over time configurations. The force \vec{F}_{ij} of Eq. 2 on each particle has three contributions [19] resulting from the coarse-graining procedure: a *conservative* component \vec{F}_{ij}^C , a *dissipative* component \vec{F}_{ij}^D and a *stochastic* one \vec{F}_{ij}^S . All these forces are pair-wise, to guarantee momentum conservation, and limited to a cut-off radius r_c .

The conservative soft-core repulsive force has the following expression:

$$\vec{F}_{ij}^C = \begin{cases} a_{\alpha,\beta} \left(1 - \frac{r_{ij}}{r_c}\right) \hat{r}_{ij} & r_{ij} \leq r_c, \\ 0 & r_{ij} > r_c \end{cases} \quad (3)$$

with $\vec{r}_{ij} = \vec{r}_i - \vec{r}_j$ is the vector distance between the i -th and j -th particle, $r_{ij} = |\vec{r}_{ij}|$ and $\hat{r}_{ij} = \vec{r}_{ij}/r_{ij}$. Such repulsive potential models the averaged fast microscopic length and time scales and was first derived by coarse-graining particles interacting via a Lennard-Jones potential [33]. The indexes α, β indicates the particle type (solvent or polymer, in our case). The constant $a_{\alpha,\beta}$ measures the force between two completely overlapping particles and it is casted from the compressibility of the modeled fluid.

The two other forces account for the loss of details in the coarse-graining procedure. The dissipative force has the form:

$$\vec{F}_{ij}^D = -\gamma w^D(r_{ij}) (\hat{r}_{ij} \cdot \vec{v}_{ij}) \hat{r}_{ij}, \quad (4)$$

where the standard choice in literature for the "weight function" $w^D(r_{ij})$ is:

$$w^D(r_{ij}) = \begin{cases} \left(1 - \frac{r_{ij}}{r_c}\right) \hat{r}_{ij} & r_{ij} \leq r_c, \\ 0 & r_{ij} > r_c. \end{cases} \quad (5)$$

Equation (4) introduces a friction among particles proportional to the relative velocity $\vec{v}_{ij} = \vec{v}_i - \vec{v}_j$. Thermal fluctuations are added via the stochastic force:

$$\vec{F}_{ij}^S = \sigma w^S(r_{ij}) \theta_{ij} (\Delta t)^{-\frac{1}{2}} \hat{r}_{ij} \quad (6)$$

where σ is a constant (related to temperature), $w^S(r_{ij})$ is a weight function and θ_{ij} is a random number extracted from a gaussian distribution with zero average and independent in time and among particle pairs: $\langle \theta_{ij}(t) \theta_{lm}(t') \rangle = (\delta_{il} \delta_{jm} + \delta_{im} \delta_{jl}) \delta(t - t')$. Momentum conservation requires $\theta_{ij} = \theta_{ji}$.

Two additional constraints, $w^D(r_{ij}) = [w^R(r_{ij})]^2$ and $\gamma = \frac{\sigma^2}{2k_B T}$, guarantee that the probability distribution respects the statistics of the NVT ensemble [20].

To mimic the brush chains we add a finite extensible nonlinear elastic potential (FENE) [34]

$$\vec{F}_{ij}^{fene} = -2kR^2 \frac{r_{ij} - r_{eq}}{R^2 - (r_{ij} - r_{eq})^2} \hat{r}_{ij} \quad r_{ij} - r_{eq} < R \quad (7)$$

which account for the neighbour particle connectivity. In Eq. (7), r_{eq} is the equilibrium distance between neighbour monomers and R is the maximum allowed extensibility. Grafted points are randomly chosen from a uniform distribution and located on a flat surface. Note that polymers are non-ideal since they interact via an excluded volume potential.

1.1 DPD and physical units

We chose the DPD units such as $r_c = 1$, $m_i = 1$, $t_{DPD} = 1$ and $k_B T = 1$. Following [19], we fix the solvent-solvent interaction parameter a_{SS} relating it to the adimensional compressibility of water κ_T^{-1} . A comparison between the equation of state of a simulated DPD system and the experimental data ($\kappa_T^{-1}(water) = 16$ at room temperature) suggests $a_{SS} = 75k_B T / \rho = 25$. We assume that the polymer-polymer interaction parameter has the same value (e.g. $a_{SS} = a_{PP}$), while we select a smaller value for the solvent-polymer parameter $a_{SP} = 20$ (*good solvent* conditions). The noise amplitude is fixed to $\sigma = 3$. For the FENE potential, finally, we use $r_{eq} = 0.86$, $R = 1$ and $k = 50$.

In DPD the choice for the physical units depends on the level of coarse-graining is desired. Our reference system is the endothelial glycocalyx, therefore we fix the physical lengthscale l_{phys} relating the spacing between different filaments of the glycocalyx network, $d_{glyco} = 20nm$ [35] with the average distance between anchor points of our brush, $d_{graft} = \sqrt{1/\sigma_{graft}} = 0.82$:

$$l_{phys} = d_{glyco} / d_{graft} = 24 \cdot 10^{-9} m.$$

We underline that with this choice also the brush thickness is in the range of endothelial glycocalyx ($100nm \div 1000nm$ [36]).

As for the physical mass scale m_{phys} and physical time scale t_{phys} , we exploit the comparison between viscosities and between energies. The viscosity of water η_{phys} is $\eta_{phys} = 10^{-3} Pa \cdot s$ at $300K$ and the DPD viscosity η_{DPD} in a bare channel, estimated from the slit-pore velocity profile relation $\eta = \rho A (L_z/2)^2 / 2v_{max}$, where v_{max} is the maximum velocity (see Sect. 1.2 for definitions of the other parameters), corresponds in our case to $\eta_{DPD} = 0.84$. The physical energy scale is defined as $k_B T_{phys}$, with $T_{phys} = 300K$. Thus we can write down two relations

$$m_{phys} = \frac{\eta_{phys}}{\eta_{DPD}} t_{phys} l_{phys},$$

$$t_{phys} = \frac{l_{phys}}{v_{phys}} = \frac{l_{phys}}{\sqrt{\frac{3k_B T_{phys}}{m_{phys}}}},$$

from which we extract

$$t_{phys} = \frac{l_{phys}^3}{3k_B T_{phys}} \frac{\eta_{phys}}{\eta_{DPD}} = 1.8 \cdot 10^{-6} s,$$

$$m_{phys} = \frac{\eta_{phys}}{\eta_{DPD}} t_{phys} l_{phys} = 5.1 \cdot 10^{-17} Kg.$$

1.2 The system geometry

We simulate a parallelepiped box of sides $L_x = 30$, $L_y = 5$ and $L_z = 50$. On the x - and y - axes we impose periodic boundary conditions, while at $z = 0$ and $z = L_z$ two impenetrable parallel walls of infinite mass are set. At the wall we use the so-called ‘‘bounce back reflection’’ conditions [37] in which all the velocity components are reversed:

$$\vec{v} \rightarrow -\vec{v} \quad \text{at} \quad z = 0, L_z. \quad (10)$$

Such conditions assure no-slip boundaries. The integration time step is $\Delta t = 0.02$. We set the density $\rho = N/(L_x L_y L_z) = 3$ [19], therefore $N = 22500$. We fix the number of monomers per chain $n = 40$ and the grafting density $\sigma_{graft} = 1.5$, defined as $\sigma_{graft} = N_{ch}/(L_x L_y)$, with N_{ch} the number of chains composing the brush. For the sake of ease and computational time, we attach polymers only at the bottom wall.

In order to produce a parabolic velocity profile inside the channel (e.g. along the z direction) a constant acceleration $\vec{A} = A\hat{x}$ is applied to all fluid particles:

$$m_i \dot{\vec{v}}_i^{fluid} = \vec{F}_{ij}^{fluid} + m_i \vec{A}. \quad (11)$$

In turn, these fluid particle exchange moment with the chains, dragging them. Different values of A allow us to probe different dynamic regimes.

2. BRUSH EQUILIBRIUM PROPERTIES

Polymer brushes immersed in a liquid at equilibrium (i.e. in the absence of flow) have been thoroughly investigated in the past [38–41]. Here we recall that the brush equilibrium conformation results from the balance between configurational entropy, that tends to make chains visit the whole available space, and excluded volume interactions, avoiding contact between monomers. The brush can be properly described by its profile $\rho(z)$, indicating the probability distributions of finding a monomer at distance z from the grafting wall. We show in Fig. 7 $\rho(z)$ at fixed $\sigma_{graft} = 1.5$ for several chain lengths ($n = 20, 25, 30, 36, 40, 45$). In line with previous theoretical results [39] and numerical studies [40, 42], the higher the volume fraction, the more step-like the density profile is.

A definition of the brush height h in term of the first moment $\langle z \rangle$ of the density profile depends on the shape of $\rho(z)$. Assuming that each chain is completely elongated so that free ends are all at the maximum distance from the grafting wall, the profile $\rho(z)$ is step-like (*Alexander model*) and the brush height can be defined as $h = 2 \langle z \rangle$. A less rigid theory (*self-consistent field theory*) hypothesizes that monomers of a same chain are distributed as a random walk, therefore the free end position ranges uniformly over the whole brush thickness. In such a case the profile is parabolic, $\rho(z) = \rho(0)(1 - z^2/h^2)$, and the brush height h is $h = \frac{8}{3} \langle z \rangle$. For the simulations discussed in the manuscript we select $n = 40$, so that the evaluated $\rho(z)$ is in between the step and the parabolic shapes (see Fig. 7). In the following, we define h following the definition of a step distribution, e.g.

$$h = 2 \frac{\int_0^\infty z \rho(z) dz}{\int_0^\infty \rho(z) dz} \quad (12)$$

2.1 Brush compression properties

From simulations at equilibrium ($A = 0$) in which the brush is compressed by a flat surface kept at a fixed position S_{fix} we have estimated the Young’s modulus E as $E = \frac{P}{\Delta S/S_0}$. In this expression, $\Delta S/S_0 = (S_{fix} - S_0)/S_0$ is the compression of the brush relative to the value S_0 indicating the brush surface without any imposed confinement and P is the pressure exerted by polymers on the pressing apparatus. In Fig. 8 we observe that E is increasing with the compression. We now notice that flow produces a compression of the brush (see Fig. 9). Equating the compression imposed at equilibrium with the one produced by the applied flow (shaded areas in Fig. 8) we

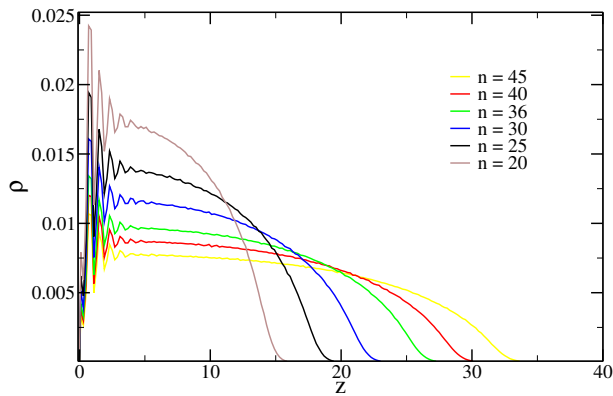


FIG. 7. Probability distributions of polymer brushes at equilibrium: fixed the grafting density, $\sigma_{graft} = 1.5$, we varied the degree of polymerization n . The case $n = 40$ corresponds to an almost step-like profile $\rho(z)$.

conclude that the brush elastic response is modified by a change in Wi .

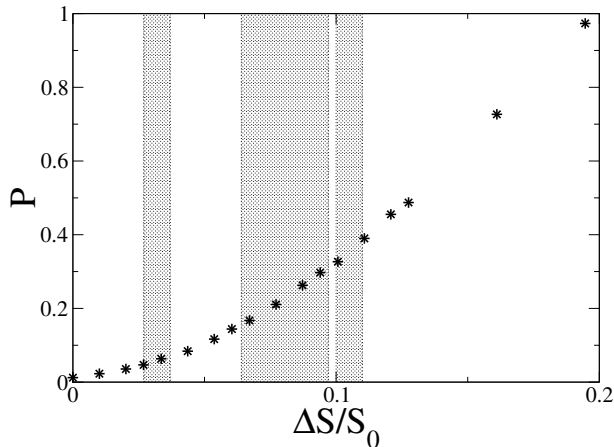


FIG. 8. The brush elastic response stored in the Young's modulus E . The modulus is defined as the coefficient between the relative brush compression and the applied pressure needed to produce it. The shaded areas indicate the ranges of brush surface compression corresponding to the three regions of flow inversion.

3. THE WEISSENBERG NUMBER

Instead of using A as a measure of the flow intensity we prefer to introduce an adimensional quantity, the Weissenberg number $Wi := t_{brush}/t_{flow}$, where t_{brush} should be a characteristic structural time of the unperturbed brush and t_{flow} should provide an estimate of the typical time scale associated to the flow. We evaluate t_{brush} as the relaxation time obtained by the decay of the autocorrelation function, averaged over all distinct polymers, of the end-to-end vector amplitude $R_{ee} = |\vec{r}_0 - \vec{r}_n|$,

Conversion $A \leftrightarrow Wi$

A	Wi	A	Wi	A	Wi	A	Wi
0.005	45	0.022	208	0.047	409	0.064	612
0.007	64	0.023	218	0.048	413	0.065	616
0.01	91	0.028	275	0.05	418	0.066	627
0.015	137	0.03	297	0.051	420	0.067	642
0.016	147	0.034	340	0.055	430	0.07	737
0.017	158	0.037	375	0.0565	588	0.075	788
0.018	167	0.04	400	0.575	593	0.08	832
0.019	175	0.043	405	0.058	595	0.1	1044
0.02	187	0.045	406.7	0.06	599		
0.021	200	0.046	407.4	0.063	607		

TABLE I. Tables of conversions between the constant acceleration A , imposed on each solvent particle to obtain a parabolic velocity profile, and the estimated a -dimensional Weissenberg number Wi .

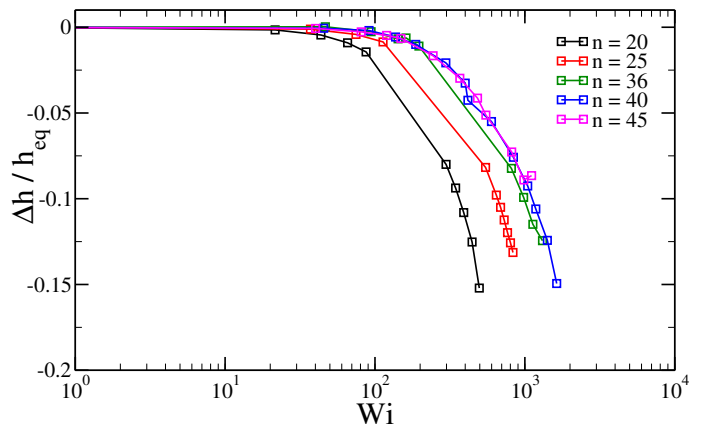


FIG. 9. The brush height h relative to the equilibrium value h_{eq} as function of Wi . The brush height is defined in section 2. For $Wi < 100$ the height keeps basically constant, while for $Wi > 100$ the flow has the effect to compress the brush.

where \vec{r}_n and \vec{r}_0 are the position vectors of, respectively, the last particle and the anchor of one chain inside the brush. According to such definition, the relaxation time t_{brush} assumes a dependency on the grafting density and on the degree of polymerization, thus representing a time scale of the whole brush rather than an isolated single-chain property. The R_{ee} auto-correlation function can be well represented by a stretched exponential decay $R_{ee} \sim e^{-(t/t_o)^\beta}$, where t_o is the characteristic time scale and β the so-called stretching exponent. Thus $t_{brush} = \Gamma[1/\beta]t_o/\beta$. For $\sigma_{graft} = 1.5$ and $n = 40$ we obtain $t_{brush} = 1746$. Regarding t_{flow} , we choose the inverse of the averaged shear rate $\dot{\gamma}$ calculated as the ratio between the maximum flow velocity v_{max} in the channel and the corresponding z -coordinate R . Since our brush under flow experiences compression (see Fig. 9) and polymers are set only at the bottom wall, both v_{max} and R depend on the imposed acceleration A .

In table Tab. I we list the correspondences between each value of A and its Wi .

4. VIDEOS

We show in movies SI1 and SI2 the dynamics of a single chain inside the brush for two different Wi , one giving flow inversion (movie SI1) and the other with no flow inversion (movie SI2): the recursive motion is constituted by an alternation of elongation-stretching-recoiling in both cases, thus it cannot be used as sufficient explanation for the backflow phenomenon.

The motion of the whole brush under flow has been recorded in movies SI3 and SI4. In the first case no collective motion is detectable and no backward flow is observed in the velocity profile, while in the second case there is concurrence of a surface wave and of flow inversion.

5. FINITE SIZE EFFECT

We have investigated the influence of finite size effect increasing the channel length L_x at fixed acceleration A : the wave persists. For a larger channel, $30 < L_x < 40$, the wave increases in wavelength ($\lambda = L_x$) and decreases in frequency, as shown in Fig. 10, such that the propagation speed keeps constant. The wave amplitude decreases and, in accordance with the Taylor's relation (see Letter, Eq. (1)), v_{min} decreases too.

Another test has been attempted increasing, up till the double, both L_x and L_z ($L_x = 60$ and $L_z = 100$). For such a system we found again, for $Wi = 464$, a surface wave, with double amplitude and double wavelength (see movie SI5). However, investigating channels up to $L_x = 360$, $L_y = 20$ and $L_z = 150$, we found that the amplitude of the surface wave does not keep on growing upon increasing L_x : in fact, its value seems to reach a plateau. We interpret this non-linear behaviour as a consequence of the finite extensibility of the polymers, e.g. due to the higher and higher energy required to significantly compress and stretch the brush.

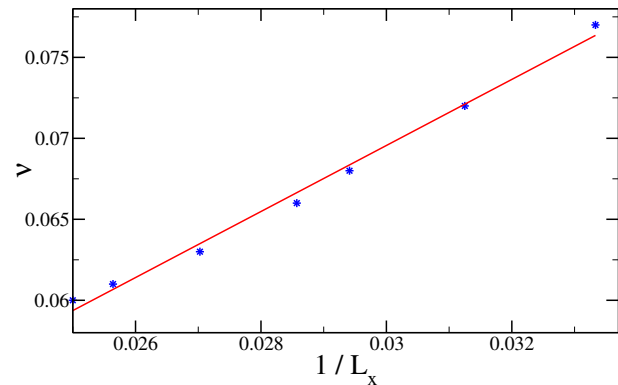


FIG. 10. Increasing the channel length L_x , $30 < L_x < 40$, at fixed acceleration $A = 0.05$ the wave increases in wavelength ($\lambda = L_x$) and decreases in frequency such that the propagation speed keeps constant.

* sofia.biagi@ujf-grenoble.fr

[1] P. Pincus, *Macromolecules* **24**, 2912 (1991).
 [2] F. Lo Verso, S. A. Egorov, A. Milchev, and K. Binder, *The Journal of Chemical Physics* **133**, 184901 (2010).
 [3] B. Jaquet, D. Wei, B. Reck, F. Reinhold, X. Zhang, H. Wu, and M. Morbidelli, *Colloid and Polymer Science* **291**, 1659 (2013).
 [4] M. Kobayashi, H. Tanaka, M. Minn, J. Sugimura, and A. Takahara, *ACS Appl. Mater. Interfaces* **6**, 20365 (2014), pMID: 25340883, <http://dx.doi.org/10.1021/am505906h>.
 [5] J. Klein, E. Kumacheva, D. Mahalu, D. Perahia, and L. Fetters, *Nature* **370**, 634 (1994).
 [6] M. Chen, W. Briscoe, S. Armes, and J. Klein, *Science* **323**, 1698 (2009).

[7] S. N. Ramakrishna, R. M. Espinosa-Marzal, V. V. Naik, P. C. Nalam, and N. D. Spencer, *Langmuir* **29**, 15251 (2013).
 [8] L. Landherr, C. Cohen, P. Agarwal, and L. Archer, *Langmuir* **27**, 9387 (2011).
 [9] S. Weinbaum, J. M. Tarbell, and E. R. Damiano, *Annual Review of Biomedical Engineering* **9**, 121 (2007).
 [10] S. Reitsma, D. Slaaf, H. Vink, M. van Zandvoort, and M. oude Egbrink, *Pflugers Arch.* **454** (2007).
 [11] M. Nieuwdorp, M. C. Meuwese, H. Vink, J. B. Hoekstra, J. J. Kastelein, and E. S. Stroes, *Current Opinion in Lipidology* **16**, 507 (2005).
 [12] E. P. Schmidt, Y. Yang, W. J. Janssen, A. Gandjeva, M. J. Perez, L. Barthel, R. L. Zemans, J. C. Bowman, D. E. Koyanagi, Z. X. Yunt, L. P. Smith, S. S. Cheng, K. H. Overdier, K. R. Thompson, M. W. Geraci, I. S. Douglas, D. B. Pearse, and R. M. Tuder, *Nat Med* **18**, 1217 (2012).
 [13] C. Murphy and V. Turner, *Journal of Anatomy* **17**, 109 (1991).
 [14] B. Button, L.-H. Cai, C. Ehre, M. Kesimer, D. B. Hill, J. K. Sheehan, R. C. Boucher, and M. Rubinstein, *Science* **337**, 937 (2012), <http://www.sciencemag.org/content/337/6097/937.full.pdf>.
 [15] T. W. Secomb, R. Hsu, and A. R. Pries, *American Journal of Physiology - Heart and Circulatory Physiology* **281**, H629 (2001).
 [16] S. Weinbaum, X. Zhang, Y. Han, H. Vink, and S. C. Cowin, *Proceedings of the National Academy of Sciences* **100**, 7988 (2003).
 [17] L. Lanotte, S. Guido, C. Misbah, P. Peyla, and L. Bureau, *Langmuir* **28**, 13758 (2012).
 [18] P. Hoogerbrugge and J. M. V. A. Koelman, *Europhysics Letters* **19**, 155 (1992).
 [19] R. D. Groot and P. B. Warren, *The Journal of Chemical Physics* **107**, 4423 (1997).
 [20] P. Español and P. B. Warren, *Europhysics Letters* **30**, 191 (1995).
 [21] J. Ilytskyi, S. Sokolowski, and T. Patsahan, *Condensed Matter Physics* **16**, 13606 (2013).
 [22] F. Léonforte, J. Servantie, C. Pastorino, and M. Müller, *Journal of Physics Condensed Matter* **23**, 184105 (2011).
 [23] M. Müller and C. Pastorino, *EPL (Europhysics Letters)*

- 81**, 28002 (2008).
- [24] M. Deng, X. Li, H. Liang, B. Caswell, and G. E. Karniadakis, *Journal of Fluid Mechanics* **711**, 192 (2012).
- [25] G. Taylor, *Proceedings of the Royal Society of London. Series A. Mathematical and Physical Sciences* **209**, 447 (1951).
- [26] J. Elgeti and G. Gompper, *Proceedings of the National Academy of Sciences* **110**, 4470 (2013).
- [27] J. R. Blake, *Journal of Fluid Mechanics* **55**, 1 (1972).
- [28] F. Gosselin and E. de Langre, *European Journal of Mechanics-B/Fluids* **28**, 271 (2009).
- [29] V. V. Babenko, H. H. Chun, and I. Lee, *Boundary Layer Flow over Elastic Surfaces*, edited by V. V. B. H. C. Lee (Butterworth-Heinemann, Oxford, 2012).
- [30] S. Mandre and L. Mahadevan, *Proceedings of the Royal Society of London A: Mathematical, Physical and Engineering Sciences* (2009), 10.1098/rspa.2009.0328.
- [31] R. M. Fuchsli, H. Fellermann, A. Eriksson, and H.-J. Ziock, *The Journal of chemical physics* **130**, 214102 (2009).
- [32] D. Frenkel and B. Smit, *Understanding Molecular Simulation: From Algorithms to Applications*, Computational science series (Elsevier Science, 2001).
- [33] B. M. Forrest and U. W. Suter, *The Journal of Chemical Physics* **102**, 7256 (1995).
- [34] G. S. Grest and K. Kremer, *Physical Review A* **33**, 3628 (1986).
- [35] S. Weinbaum, J. M. Tarbell, and E. R. Damiano, *Annual Review of Biomedical Engineering* **9**, 121 (2007).
- [36] B. Fu and J. Tarbell, *Wiley Interdiscip Rev Syst Biol Med* **5**, 381 (2013).
- [37] M. Revenga, I. Zúñiga, and P. Español, *Computer Physics Communications* **121-122**, 309 (1999).
- [38] S. T. Milner, T. A. Witten, and M. E. Cates, *EPL (Europhysics Letters)* **5**, 413 (1988).
- [39] S. T. Milner, *Science* **251**, 905 (1991).
- [40] K. Binder, T. Kreer, and A. Milchev, *Soft Matter* **7**, 7159 (2011).
- [41] J. L. Barrat, *Macromolecules* **25**, 832 (1992).
- [42] C. Pastorino, K. Binder, T. Kreer, and M. Müller, *The Journal of Chemical Physics* **124** (2006).